

# Stellar and gaseous abundances in M 82<sup>1</sup>

L. Origlia

INAF - Osservatorio Astronomico di Bologna, Via Ranzani 1, I-40127 Bologna, Italy,  
origlia@bo.astro.it

P. Ranalli

Dipartimento di Astronomia Università di Bologna, Via Ranzani 1, I-40127 Bologna, Italy,  
ranalli@bo.astro.it

A. Comastri

INAF - Osservatorio Astronomico di Bologna, Via Ranzani 1, I-40127 Bologna, Italy,  
comastri@bo.astro.it

and

R. Maiolino

INAF - Osservatorio Astronomico di Arcetri, Largo E. Fermi 5, I-50125 Firenze, Italy,  
maiolino@arcetri.astro.it

## ABSTRACT

The near infrared (IR) absorption spectra of starburst galaxies show several atomic and molecular lines from red supergiants which can be used to infer reliable stellar abundances. The metals locked in stars give a picture of the galaxy metallicity prior to the last burst of star formation. The enrichment of the new generation of stars born in the last burst can be traced by measuring the hot gas in the X-rays. For the first time detailed stellar abundances in the nuclear region of the starburst galaxy M 82 have been obtained. They are compared with those of the hot gas as derived from an accurate re-analysis of the XMM-Newton and Chandra nuclear X-ray spectra. The cool stars and the hot gas suggest  $[\text{Fe}/\text{H}] = -0.35 \pm 0.2$  dex, and an overall  $[\text{Si}/\text{Mg}/\text{Fe}]$  enhancement by  $+0.4$  and  $+0.5$  dex, respectively. This is consistent with a major chemical enrichment by

---

<sup>1</sup>Based on observations with the Near Infrared Camera Spectrometer (NICS) mounted at the Telescopio Nazionale Galileo (TNG), La Palma, Spain and archival XMM-Newton and Chandra data.

SN e II explosions in recursive bursts on short time scales. Oxygen is more puzzling to interpret since it is enhanced by  $\sim 0.3$  dex in stars and depleted by  $\sim 0.2$  dex in the hot gas. None of the standard enrichment scenarios can fully explain such a behavior when compared with the other elements.

Subject headings: galaxies: individual (M 82) | galaxies: abundances | galaxies: starburst | X-ray: galaxies | infrared: galaxies

## 1. Introduction

The signature of the star formation (SF) history of a galaxy is imprinted in the abundance patterns of its stars and gas. Determining the abundance of key elements released in the interstellar medium (ISM) by stars with different mass progenitors and hence on different time scales, will thus have a strong astrophysical impact in drawing the global picture of galaxy formation and evolution (McWilliam 1997).

So far, the metallicities of distant starburst (SB) galaxies have been mainly derived by measuring the nebular lines associated to their giant H II regions (Storchi-Bergmann, Calzetti & Kinney 1994; Ciolet al. 1999; Henry, Edmunds & Koppén 2000). Direct determination of O and N abundances can be obtained once electron temperature ( $T_e$ ) is well established (McCall 1984). At high metallicities  $T_e$  decreases due to strong lines cooling and its major diagnostic (the weak [O III]  $\lambda 4366$ ) is no longer observable. Several alternative methods based on other strong lines were proposed in the past years (Page et al. 1979; Dopita & Evans 1986; McGaugh 1991) to derive  $T_e$ , but all of them rely on a large number of physical parameters and model assumptions for the geometry and the nature of the ionizing populations (c.f. e.g. Stasinska (2001) for a review). Depending on the adopted calibrations, quite different abundance sets can reproduce the observed line ratios.

However, abundances in SB galaxies can be also measured from absorption stellar features in the near IR and/or emission lines in the hot X-ray gas. Stellar abundances can be poorly constrained from optical spectra, since the nebular emission strongly dilutes the absorption lines and dust can heavily obscure the central regions where most of the burst activity is concentrated. On the contrary, in the near IR the stellar continuum due to red supergiants (RSGs) usually largely dominates over the possible gas and dust emission (Olive & Origlia 1998; Origlia & Olive 2000). The X-ray emission from SB galaxies at  $E > 2$  keV is mainly due to high mass X-ray binaries with power-law spectra, while at lower energies hot plasma mainly heated by SN explosions (Dahlem et al. 1998) dominates and the resulting spectrum is a superposition of thermal continuum and emission lines from atomic

recombinations (Fabbiano 1989; Persic & Rephaeli 2002).

Determining the abundances of SB galaxies is not only relevant to constrain their SF history, but also offers the unique chance of directly witnessing the enrichment of the ISM (see e.g. Mader & Conti 1994, for a review). Metals locked into stars give a picture of the enrichment just prior to the last burst of SF, while the hot gas heated by SNe II explosions should trace the enrichment by the new generation of stars. Nebular metallicities from the cold gas should potentially trace the stellar ones if the cooling and mixing timescales are slow (up to 1 Gyr), as suggested by some models (see e.g. Tenorio-Tagle 1996) since the gas enriched by the ongoing burst is still too hot to be detected in the optical lines. On the contrary, if rapid (a few Myr) cooling and mixing occur as suggested by other models (see e.g. Recchi, Matteucci & D'Ercolo 2001), the nebular abundances could trace the gas enriched by the new population of stars (similarly to X-rays). Hence, important constraints on the cooling and mixing timescales of the gas can be provided by comparing the metallicity inferred from stars and hot plasma with those of the cold gas.

Sect. 2 briefly reviews the nebular abundance estimates of M 82, as published so far in the literature. Sect. 3 shows our near IR spectra of the nuclear region of M 82 and the derived stellar abundances. Sect. 4 presents a re-analysis of the XMM-Newton and Chandra nuclear X-ray spectra and the hot gas phase abundances. Sect. 5 summarizes the overall chemical enrichment scenario in M 82 as traced by the stellar, cold and hot gas-phase abundances, while in Sect. 6 we draw our conclusions.

## 2. Nebular abundances of M 82 from the literature

M 82 is a prototype of SB galaxies (Rieke et al. 1980), experiencing a major SF formation episode in its nuclear regions, with strong super-wind and SN activity (Wills et al. 1999). Despite the many multiwavelength studies (see e.g. Golla, Allen & Kronberg 1996, and references therein), only few measurements of nebular abundances, mainly derived from mid/far IR forbidden lines, have been published so far. From the analysis of the [SiII] 35  $\mu$ m line in the central 300 pc in radius at the distance of M 82 (i.e.  $d \approx 3.6$  Mpc), Lord et al. (2001) suggest an indicative [Si/H]  $\approx -0.4$  dex relative to the Solar value of Grevesse & Sauval (1998).

More recently, Förster-Schreiber et al. (2001), by analyzing the nuclear spectra of M 82 taken with the Short Wavelength Spectrometer (SW S) onboard the Infrared Space Observatory (ISO) within an aperture corresponding to 100–200 pc on the sky, give cold gas-phase abundances of [Ne/H]  $\approx +0.1$ , [Ar/H]  $\approx +0.3$  and [S/H]  $\approx +0.7$  dex relative to the Solar values

of Grevesse & Sauval (1998), with an overall uncertainty between 0.2 and 0.3 dex.

By taking the line ratios listed by Alloin, Collin-Solignac, & Joly (1979) which refer to the central  $\sim 100$  pc in radius of M 82 (Peimbert & Spinrad 1970), and the empirical calibrations of McGaugh (1991) which give N and Fe abundances as a function of  $[O/H]$  (see e.g. their Figure 11, equations 9 and 10a), one can also obtain rough estimates of  $[O/H] = +0.1$ ,  $[N/H] = 0.0$  and  $[Fe/H] = -0.3$  dex relative to the Solar values of Grevesse & Sauval (1998), with an overall uncertainty of  $\sim 0.3$  dex.

The first attempt to measure hot gas-phase abundances in M 82 has been made quite recently by Ptak et al. (1997) and slightly revised by Umeda et al. (2002), by analyzing ASCA X-ray (0.4-10.0 keV) spectra. Fe and O abundances as low as 1/20 Solar and significantly higher (by a factor between 3 and 10) Si, S, Mg, Ca ones have been obtained, also consistent with BeppoSAX results (Cappi et al. 1999).

More recently, Read & Stevens (2002) by analyzing the spectra obtained with the Reflection Grating Spectrometer (RGS) onboard XMM-Newton found near-Solar Fe and O and super-Solar (between a factor of 2 and 5) Mg, Si, Ne, N abundances. While the abundance ratios are in reasonable agreement within  $\sim 0.3$  dex with Ptak et al. (1997), there is one order magnitude difference between the zero-point of the two calibrations.

### 3. IR spectra and stellar abundances

Near-IR spectroscopy is a fundamental tool to obtain accurate abundances of key elements like Fe, C, O and other metals (e.g. Si, Mg, Ca, Na, Al, Ti) in cool stars ( $T_e \lesssim 5000$  K). Several atomic and molecular lines are strong, not affected by severe blending, hence also measurable at low-medium resolution (Kleinmann & Hall 1986; Origlia et al. 1993; Wallace & Hinkle 1997; Joyce et al. 1998; Frogel et al. 2001), making them powerful abundance tracers not only in stars but also in more distant stellar clusters and galaxies and in a wide range of metallicities and ages (Origlia et al. 1997; Oliva & Origlia 1998). A abundance analysis from integrated spectra of galaxies requires full spectral synthesis techniques to properly account for line blending and population synthesis to define the dominant contribution to the stellar luminosity.

In SB galaxies the stellar IR continuum usually dominates over the possible gas and dust emission. This represents a major, conceptual simplification in population and spectral synthesis techniques, making possible and easier the interpretation of integrated spectra from distant stellar clusters and galaxies.

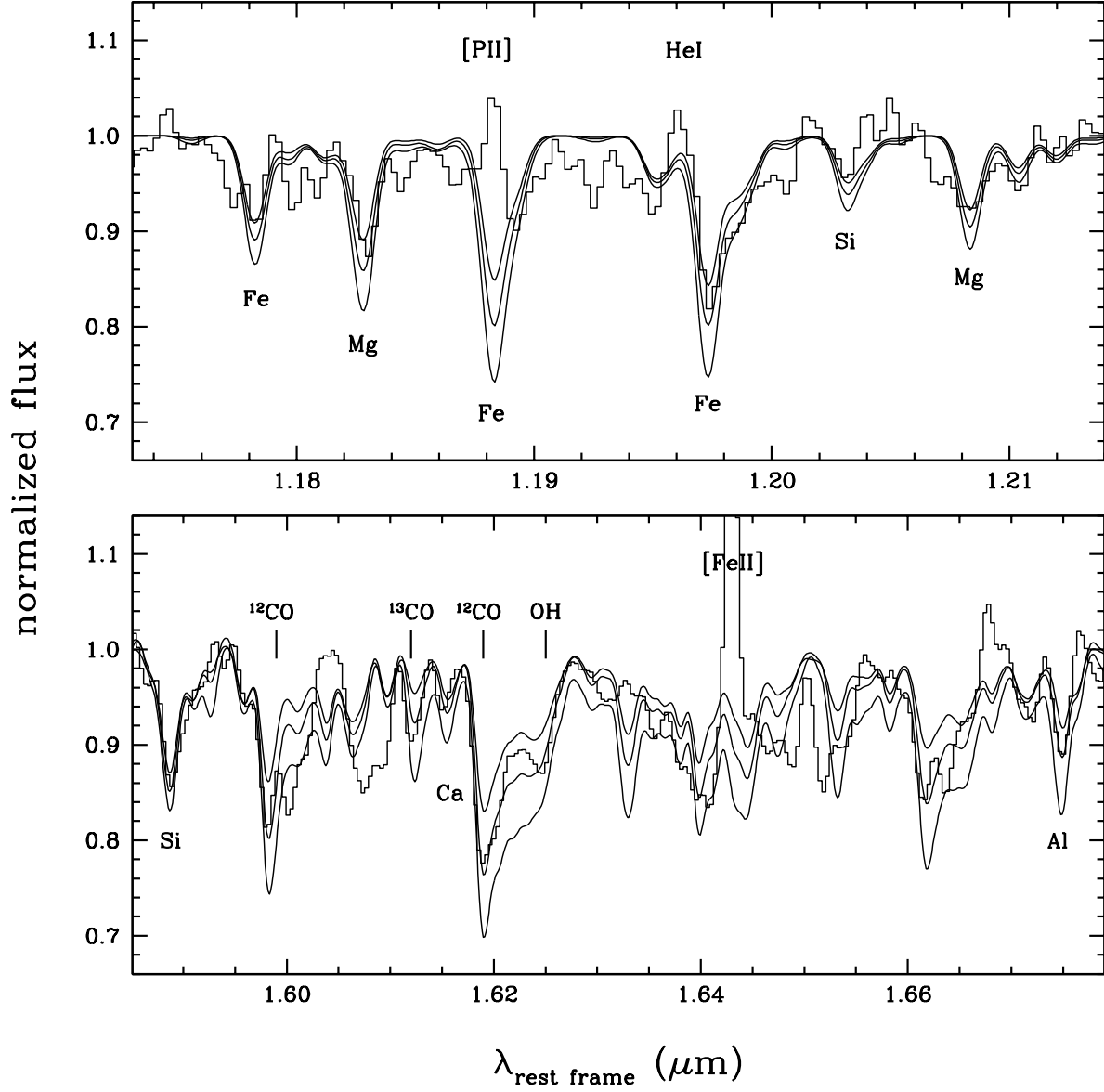


Fig. 1. | Near-IR spectra of the nuclear region of M 82. Observed spectra: histogram s; synthetic stellar best- t solution and two other models with 0.3 dex abundance variations: solid lines. A few major stellar and nebular lines are also marked.

Since the near IR continuum of SB galaxies is dominated by luminous RSGs (see e.g. Origlia & Oliva 2000, for a review), their integrated spectrum can be modeled with an equivalent, average star, whose stellar parameters (temperature  $T_{\text{eff}}$ , gravity  $\log g$  and microturbulence velocity  $v_{\text{turb}}$ ) mainly depend on the stellar age and metallicity. Both observations and evolutionary models (see e.g. Keller 1999; Origlia et al. 1999; Origlia 2003, and reference therein) suggest that RSGs of ages between  $\sim 6$  and 100 Myr and metallicities between 1/10 and Solar are characterized by low gravities ( $\log g < 1.0$ ), low temperatures ( $< 4000$  K) and relatively high microturbulence velocity ( $\sim 3$  km/s). A variation in the adopted stellar parameters for the average RSG population by  $T_{\text{eff}} = 200$  K,  $\log g = 0.5$  and  $v_{\text{turb}} = 0.5$  km s $^{-1}$  implies a  $\sim 0.1$  dex change in the abundances estimated from atomic lines, and  $\sim 0.2$  dex in those estimated from the molecular lines, which are more sensitive to stellar parameters.

1.0–1.8  $\mu$ m longslit spectra (see Fig. 1) at  $R = 2,500$  of the nuclear region of M 82 were obtained with the Near IR Camera Spectrometer (NICS) mounted at the Italian Telescopio Nazionale Galileo (TNG) on December 2002. The spectra were sky-subtracted, flat-fielded and corrected for atmospheric absorption using an O-star spectrum as reference. They were wavelength calibrated by using a Ne-Ar lamp and the monodimensional spectra were extracted by summing over the central  $0.5'' \times 3.0''$ , corresponding to an aperture projected on the source of  $9 \times 52$  pc at the distance of M 82. The spectra have been normalized to the continuum, which was determined applying a low-pass smoothing filter to each spectrum. Total integration times of 72 and 32 min in the J and H bands, respectively, were used, providing a final signal to noise ratio  $\sim 40$ .

By measuring the absorption line broadening a stellar velocity dispersion  $\sim 105 \pm 20$  km/s has been derived, in perfect agreement with the estimate by Gafney, Lester & Telesco (1993) and in the typical range of values measured in other massive SB galaxies (Oliva et al. 1999).

A grid of synthetic spectra of red supergiant stars for different input atmospheric parameters and abundances have been computed, using an updated (Origlia et al. 2002, 2003) version of the code described in Origlia et al. (1993). Briefly, the code uses the LTE approximation and is based on the molecular blanketed model atmospheres of Johnson, Bemat & Krupp (1980). It includes several thousands of near IR atomic lines and molecular roto-vibrational transitions due to CO, OH and CN. Three main compilations of atomic oscillator strengths are used, namely the Kurucz's database (c.f. <http://cfa-www.harvard.edu/amdata/ampdata/kurucz23/sekur.htm>), and those published by Biemont & Grevesse (1973) and Melendez & Barbuy (1999).

Our code provides full spectral synthesis over the 1–2.5  $\mu$ m range. Given the high degree of line blending, our abundance estimates are mainly obtained by best-fitting the full

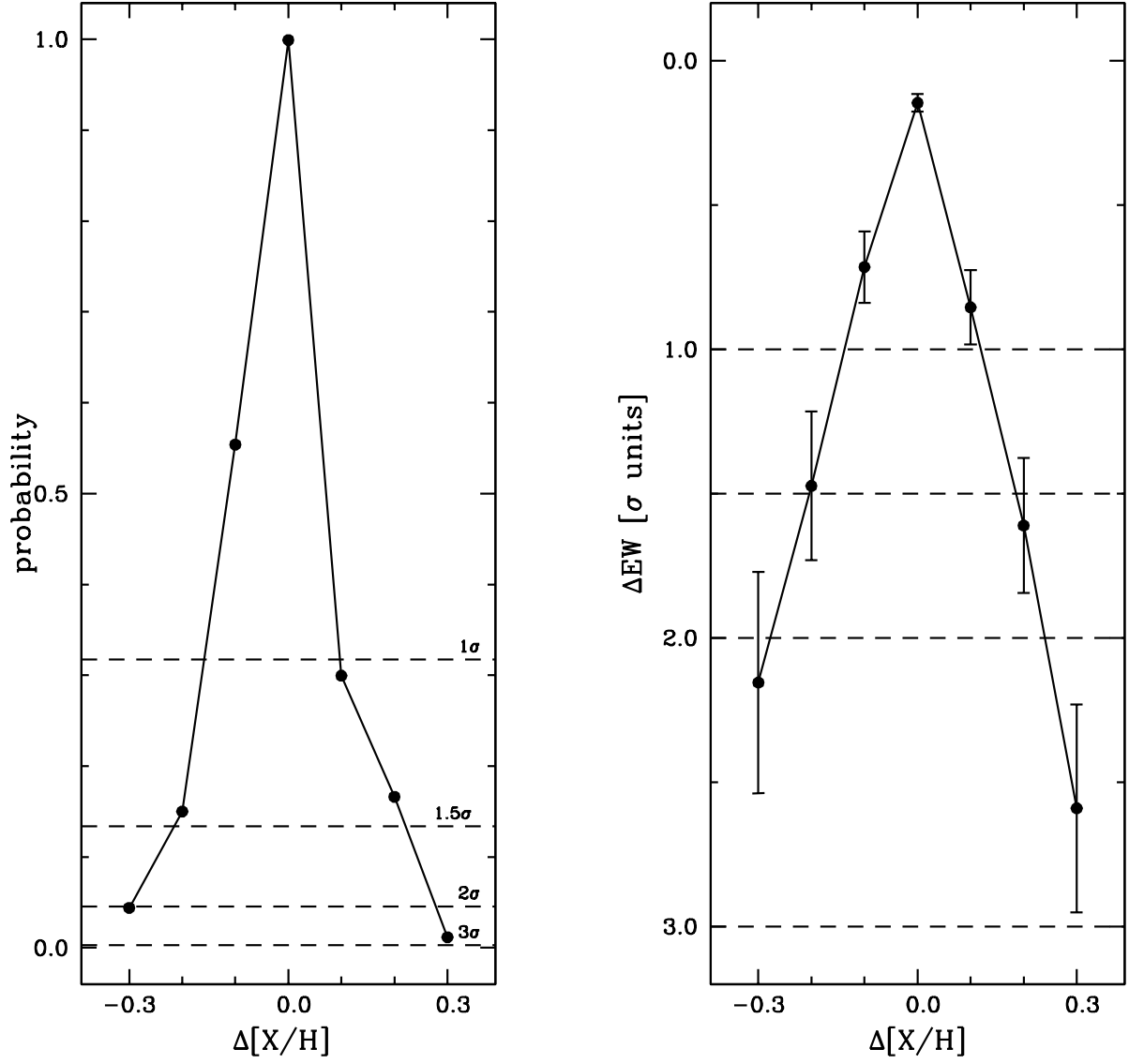


Fig. 2. | Left panel: probability of a random realization of our best-fit full spectral synthesis solution with varying the elemental abundances  $\Delta[X/H]$  of  $-0.2$  and  $0.3$  dex with respect to the best-fit (see Sect. 3). Right panel: average difference between the model and the observed equivalent widths of a few selected lines (see Sect. 3 and Fig. 1).

observed spectrum and by measuring the equivalent widths of a few selected features (cf. Fig. 1), dominated by a specific chemical element, as a further cross-check. The equivalent widths have been measured by performing a Gaussian fit with  $\sigma$  equal to the measured stellar velocity dispersion, typical values ranging between 0.5 and 3 Å, with a conservative error of 200 mÅ to also account for a 2% uncertainty in the continuum positioning.

By fitting the full observed IR spectrum and by measuring the equivalent widths of selected lines, we obtained the following best-fit stellar parameters and abundance patterns for M 82:  $T_{\text{eff}} = 4000$ ,  $\log g = 0.5$ ,  $Z = 3$ ,  $[\text{Fe}/\text{H}] = \{0.34$ ;  $[\text{O}/\text{Fe}] = +0.34$ ,  $[\text{Si}/\text{Mg}, \text{Ca}]/\text{Fe}] = +0.38$ ;  $[\text{Al}/\text{Fe}] = +0.5$ ;  $[\text{C}/\text{Fe}] = \{0.26$ ;  $^{12}\text{C}/^{13}\text{C} < 10$ . Table 3 lists the derived abundances and their associated random errors at 90% confidence. Reference Solar abundances are from Grevesse & Sauval (1998).

Synthetic spectra with lower element abundances are systematically shallower than the best-fit solution, while the opposite occurs when higher abundances are adopted. In order to check the statistical significance of our best-fit solution, as a function of merit we adopt the difference between the model and the observed spectrum (hereafter  $\Delta$ ). In order to quantify systematic discrepancies, this parameter is more powerful than the classical  $\chi^2$  test, which is instead equally sensitive to random and systematic scatters (see Origlia et al. 2003, for more details).

Since  $\Delta$  is expected to follow a Gaussian distribution, we compute  $\bar{\Delta}$  and the corresponding standard deviation ( $\sigma$ ) for the best-fit solution and 6 test models with abundance variations  $[\text{X}=\text{H}] = \{0.1, 0.2 \text{ and } 0.3 \text{ dex}$  with respect to the best-fit. We then extract 10000 random subsamples from each test model (assuming a Gaussian distribution) and we compute the probability  $P$  that a random realization of the data-points around a test model display a  $\bar{\Delta}$  that is compatible with the best-fit model.  $P < 1$  indicates that the model is a good representation of the observed spectrum.

The left panel of Fig. 2 shows the average results for the observed J and H band spectra of M 82. It can be easily appreciated that the best-fit solution provides in all cases a clear maximum in  $P$  ( $> 99\%$ ) with respect to the test models. More relevant, test models with an abundance variation  $[\text{X}=\text{H}] = \{0.2 \text{ dex}$  lie at  $P \sim 1.5$  from the best-fit solution, while test models with  $[\text{X}=\text{H}] = \{0.3 \text{ dex}$  lie at  $P \sim 2$  from the best-fit solution.

The analysis of the line equivalent widths provide fully consistent results. The right panel of Fig. 2 shows the average difference between the model and the observed equivalent width measurements. Models with  $\{0.2 \text{ dex}$  abundance variations from the best-fit solution are still acceptable at a  $P \sim 1.5$  significance level, while those with  $\{0.3 \text{ dex}$  variations are only marginally acceptable at a  $P \sim 3$  level.

Table 1. Element abundances in Solar units<sup>a</sup> as derived from our analysis of the IR and X-ray spectra.

	stellar <sup>b</sup>	hot gas-phase <sup>c</sup>
[Fe/H]	0.34 ± 0.20	0.37 ± 0.11
Fe/Fe	0.46 <sup>+0.26</sup> <sub>-0.17</sub>	0.43 <sup>+0.12</sup> <sub>-0.08</sub>
[O/H]	+0.00 ± 0.16	0.58 ± 0.19
O/O	1.00 <sup>+0.46</sup> <sub>-0.32</sub>	0.26 <sup>+0.15</sup> <sub>-0.09</sub>
[Ca/H]	+0.05 ± 0.28	{
Ca/Ca	1.11 <sup>+1.01</sup> <sub>-0.52</sub>	{
[Mg/H]	+0.02 ± 0.15	+0.13 ± 0.09
Mg/Mg	1.06 <sup>+0.44</sup> <sub>-0.31</sub>	1.36 <sup>+0.32</sup> <sub>-0.26</sub>
[Si/H]	+0.04 ± 0.28	+0.17 ± 0.08
Si/Si	1.09 <sup>+0.99</sup> <sub>-0.52</sub>	1.49 <sup>+0.32</sup> <sub>-0.26</sub>
[Al/H]	+0.23 ± 0.20	{
Al/Al	1.69 <sup>+0.97</sup> <sub>-0.62</sub>	{
[C/H]	0.60 ± 0.10	{
C/C	0.25 <sup>+0.06</sup> <sub>-0.05</sub>	{
[Ne/H]	{	0.35 ± 0.14
Ne/Ne	{	0.45 <sup>+0.17</sup> <sub>-0.12</sub>
[S/H]	{	+0.15 ± 0.13
S/S	{	1.42 <sup>+0.48</sup> <sub>-0.40</sub>

Note. | <sup>a</sup> Solar values from Grevesse & Sauval (1998).  
<sup>b</sup> Stellar abundances from TNG/NICS near IR absorption spectra of red supergiants (see Fig. 1 and Sect. 3).  
<sup>c</sup> Hot gas-phase abundances from XMM/RGS and pn spectra (see Figs. 3,5 and Sect. 4).

Models with stellar parameters varying by  $T_e = 200 \text{ K}$ ,  $\log g = 0.5$  and  $v \pm 0.5 \text{ km s}^{-1}$  and abundances varying accordingly by 0.1–0.2 dex, in order to still reproduce the deepness of the observed features, are also less statistically significant (on average only at  $2\sigma$  level) with respect to the best-fit solution. Hence, as a conservative estimate of the systematic error in the derived best-fit abundances, due to the residual uncertainty in the adopted stellar parameters, one can assume a value of  $\pm 0.1$  dex.

By taking into account the overall uncertainty in the definition of the average population and the statistical significance of our spectral synthesis procedure, we can safely conclude that the stellar abundances can be constrained well within  $\pm 0.3$  dex and their abundance ratios down to  $\pm 0.2$  dex, since some (if not all) of the stellar parameter degeneracy is removed.

#### 4. X-ray spectra and hot gas-phase abundances

The determination of the abundances of the hot X-ray emitting gas in SB galaxies has traditionally suffered from large uncertainties. Indeed, the low angular and spectral resolution of the various X-ray telescopes in the pre-XMM-Newton/Chandra era did not allow to disentangle between point sources and hot gas emission, making abundance determinations severely model-dependent (Dahlem et al. 2000). The problem lies in the fact that the X-ray spectrum of SB galaxies contains two major components: the emission from hot diffuse gas and the integrated contribution of point sources. The first is described by an optically thin thermal spectrum plus emission lines, the latter by a power-law. If the angular resolution is not good enough, it is not possible to reliably subtract the point sources from the total spectrum, so that the equivalent widths of the emission lines (and thus the element abundances) are not unambiguously defined.

On the other hand, high angular resolution alone is not enough: recent Chandra studies (Strickland et al. 2002; Martin, Kobulnicky & Heckman 2002) demonstrated that the relatively low spectral resolution of the ACIS detector makes individual element abundance analysis still problematic. The high spectral resolution of the Chandra gratings rapidly degrades for sources which are much more extended than the instrumental Point Spread Function (PSF) and thus these gratings are almost useless for the study of nearby SB galaxies. However, by coupling the high angular resolution ( $0.5''$  PSF) of Chandra with the high spectral resolution ( $\Delta E \approx 400$ ) of the XMM-EPIC, which is not sensitive to the source extension, it is possible to overcome the above described difficulties.

M 82 was observed several times by Chandra; we consider the two longest exposures, of 33 ks and 15 ks respectively, both obtained on September 1999. A cumulative spectrum of

the brightest point sources was extracted from the two Chandra ACIS-I observations; the best-fit model was an absorbed power-law with  $N_H = 7.9 \pm 0.7 \times 10^{21} \text{ cm}^{-2}$ ,  $\Gamma = 0.84 \pm 0.07$ ,  $\chi^2_r = 0.4$ , which is typical of High Mass X-ray Binaries (see Persic & Rephaeli 2002, and reference therein). The 0.5–10 keV flux was  $4.2 \times 10^{-12} \text{ erg s}^{-1} \text{ cm}^{-2}$ , which represented 25% of the total (point source plus diffuse) flux (but notice that M 82 is a variable source, Ptak & Griths 1999, Rephaeli & Gruber 2002).

M 82 was observed by XMM-Newton for 30 ks in May 2001; in the XMM-Newton observation, after light-curve cleaning,  $\sim 20$  ks of data were available for scientific analysis. We extracted the EPIC-pn spectrum from a circular region centered on the starbursting core of M 82 and with a  $15''$  radius, which approximately matches the RGS PSF; the standard recipe for EPIC spectra extraction suggested in the XMM web pages was followed. The XMMSAS software version 5.3.0 was used. A background spectrum was taken from standard background files provided by the XMM-Newton SOC. RGS spectra were extracted with standard settings (i.e. including events within 90% confidence and rejecting as background events those outside 95% of the PSF figure); this procedure is similar to the one used by Read & Stevens (2002) but with more recent calibrations. After visual inspection, we discarded the 2nd-order spectra because of low signal/noise ratio. We included in the fit only the 1st-order channels comprised in the 6–20 Å interval, since outside the S/N ratio rapidly drops. A systematic error up to 10% in the 14–18 Å channels was included (XMM calibration document XMM-SOC-CAL-TN-0030 Issue 2).

The hard-band (2–7 keV) Chandra images show that the point sources emission largely exceeds that of the hot gas, while the hard part (3–7 keV) of the pn spectrum can be well described by a power-law whose best-fit slope resulted in the same value previously determined for the Chandra point sources. Thus, making use of information from both Chandra and XMM-Newton observations, we have been able to constrain the point source slope, absorption and normalization at the moment of the XMM-Newton observation.

We jointly fitted the pn and RGS spectra with XSPEC Version 11.2 (see Fig. 3) with a two component model which is the sum of: i) an absorbed power-law (accounting for point sources) with the slope and absorption parameters fixed at the best-fit values obtained with Chandra while normalization was left free to account for variability; ii) an absorbed, optically-thin thermal plasma emission, with variable line intensities and differential emission measure (DEM) distribution. The DEM distribution was modeled with a 6<sup>th</sup> order Chebyshev polynomial (c6pvmk1 model in XSPEC); with the best-fit parameters it resembles a bell-shaped curve with a peak at  $kT = 0.7 \text{ keV}$  and  $\text{FWHM} = 0.65 \text{ keV}$  (i.e. the plasma temperatures range from 0.35 keV to 1 keV), in agreement with Read & Stevens (2002). The thermal component is absorbed by cold gas with best-fit column density  $N_H = 3.8 \times 10^{21}$

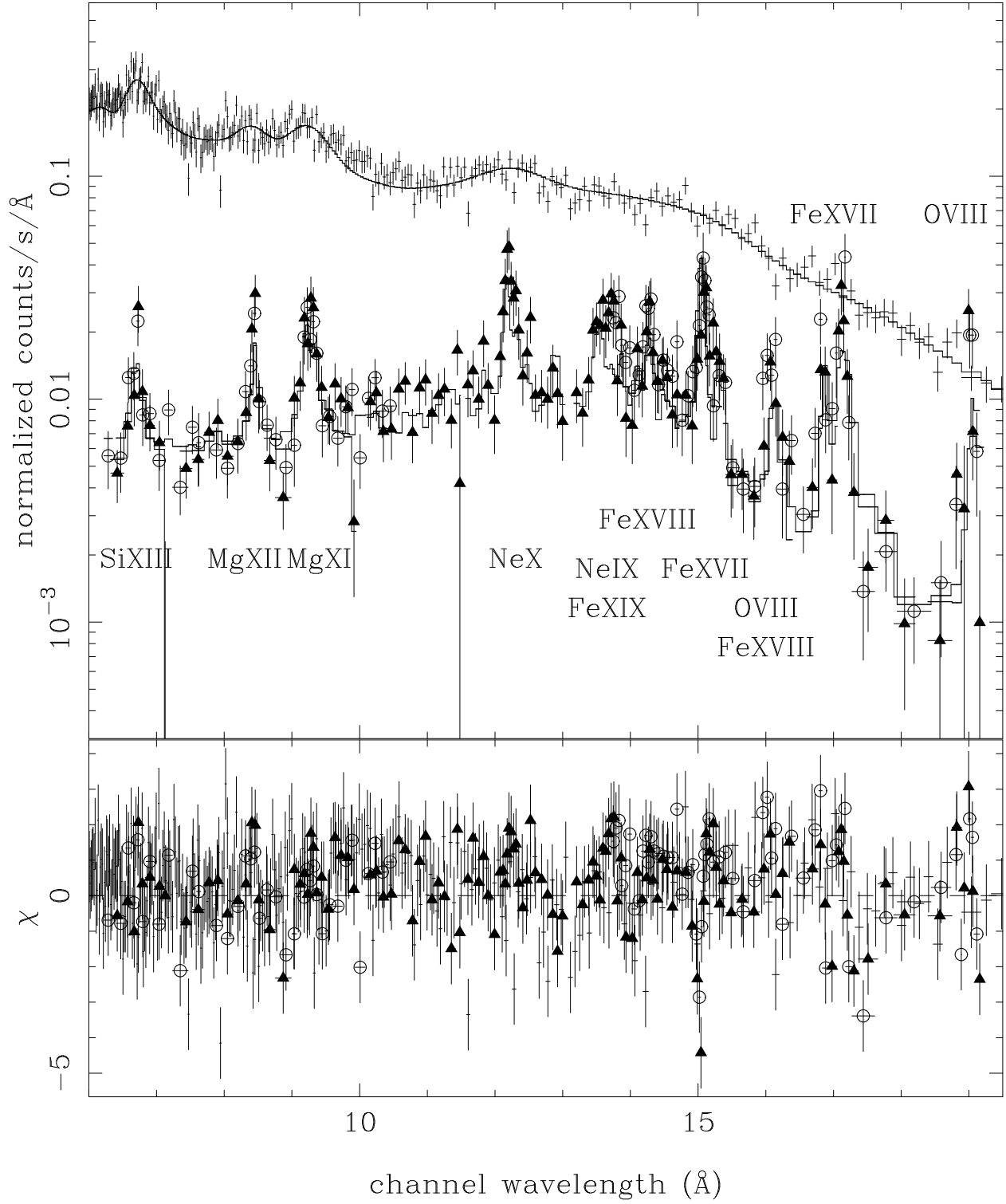


Fig. 3. | XMM-RGS spectrum of the nuclear region of M 82. Upper panel: data points (lower spectrum - open circles: RGS1; filled triangles: RGS2; upper spectrum : pn) along with the best-fit model. Lower panel: residuals in units of  $\chi$ .

cm<sup>-2</sup>.

The confidence contours of the Iron abundance versus normalization of the thermal component are reported in Fig. 4. As expected the two parameters are well correlated as the higher is the normalization of the continuum spectrum the lower is the intensity of the emission lines and in turn the element abundances. The derived abundances and their associated 90% confidence error are shown in Table 3. We notice that these abundances are about a factor 2 below those reported in Read & Stevens (2002); we attribute the discrepancy to the different modeling of the continuum emission (Read & Stevens 2002 did not include pn data, neither considered the contribution from point sources). However, it is worth of mentioning that both sets of abundances indicate a low O abundance compared to the other elements.

To further check the consistency and robustness of our estimates, we repeated the fit two times considering only the RGS data and using i) the above described thermal plus power-law model and ii) a thermal model alone. This last check, in particular, most closely matches the analysis previously made by Read & Stevens (2002) to the point that the discrepancies are within the errors and can be attributed to the differences in the used instrument calibration. The abundances derived from the three different models are plotted in Fig. 5. Those obtained combining pn and RGS have significantly smaller uncertainties. One can see that different models have mainly the effect to almost rigidly scale all the abundances, with minor impact on the abundance ratios.

The low Oxygen abundance is somehow difficult to explain in the framework of  $\alpha$ -element enhancement by type II SN explosions. Thus, to check its reliability we included in the fit also the channels corresponding to the 20-23 Å interval, where the OV II triplet is observed (although with very few counts). We find no significant difference neither in Oxygen abundance nor in DEM distribution (the OV III 19/OV II 22 ratio is extremely sensitive to the plasma temperature). Ne is also somewhat under-abundant. We checked for possible instrumental effects, such as variations in the RGS effective area in proximity of the Ne and O lines; however the effective area in this region is a rather smooth function of the wavelength, so that there should be no instrumental issues and these low abundances are likely to be real.

Since M 82 is observed edge-on, the X-ray emission of its nuclear region is subject to quite heavy absorption which could affect the O lines detected at low energies. However, as shown in Fig. 6, the contour plot of the Oxygen abundance towards the foreground absorption, suggest a rather weak correlation. In the next section we discuss other physical possibilities to explain the O under-abundance issue.

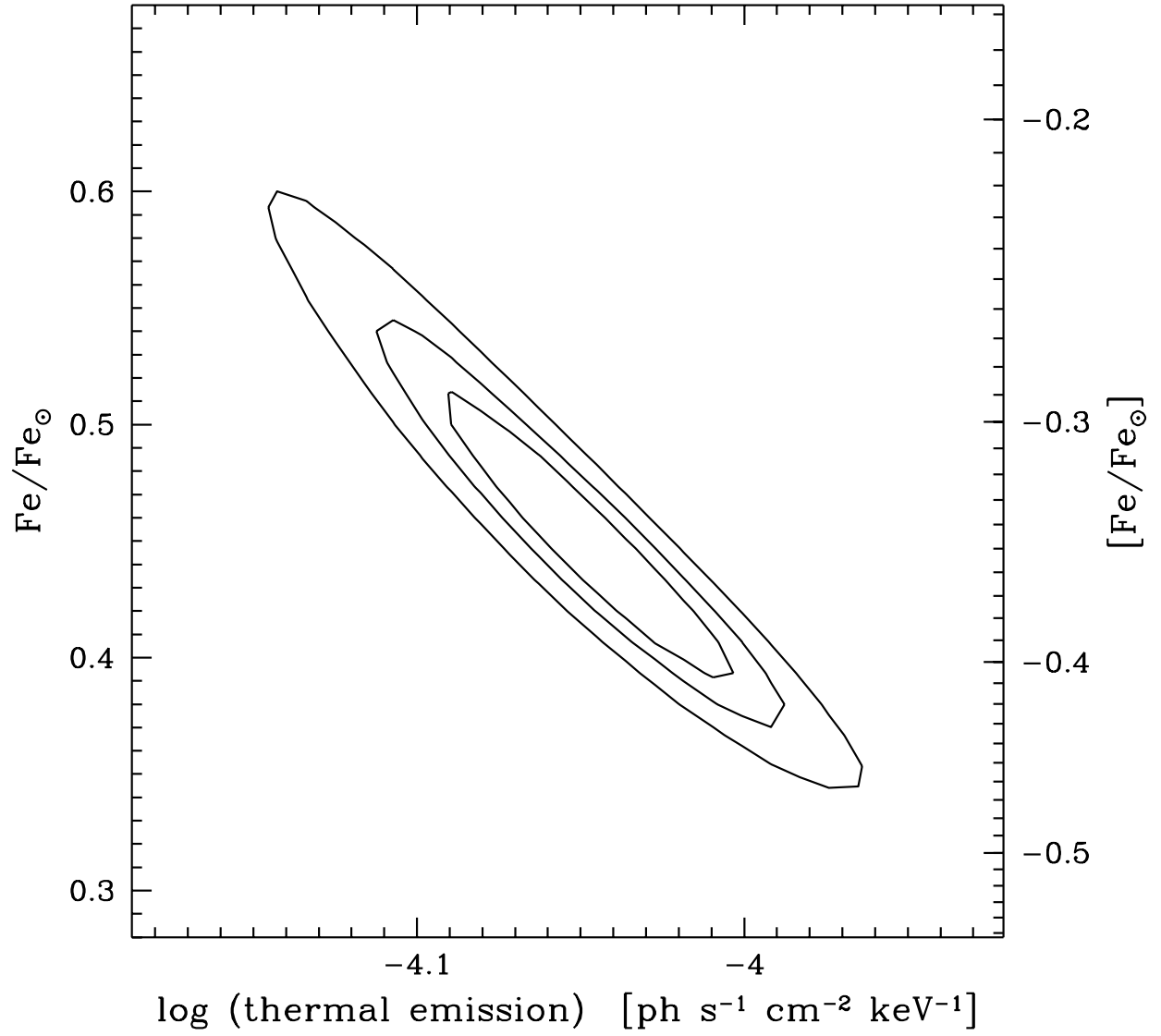


Fig. 4. | 68. 90 and 99% confidence contours of the Iron abundance vs intensity of the thermal component. For easy of reading the y-axis is shown both in linear and logarithmic scale.

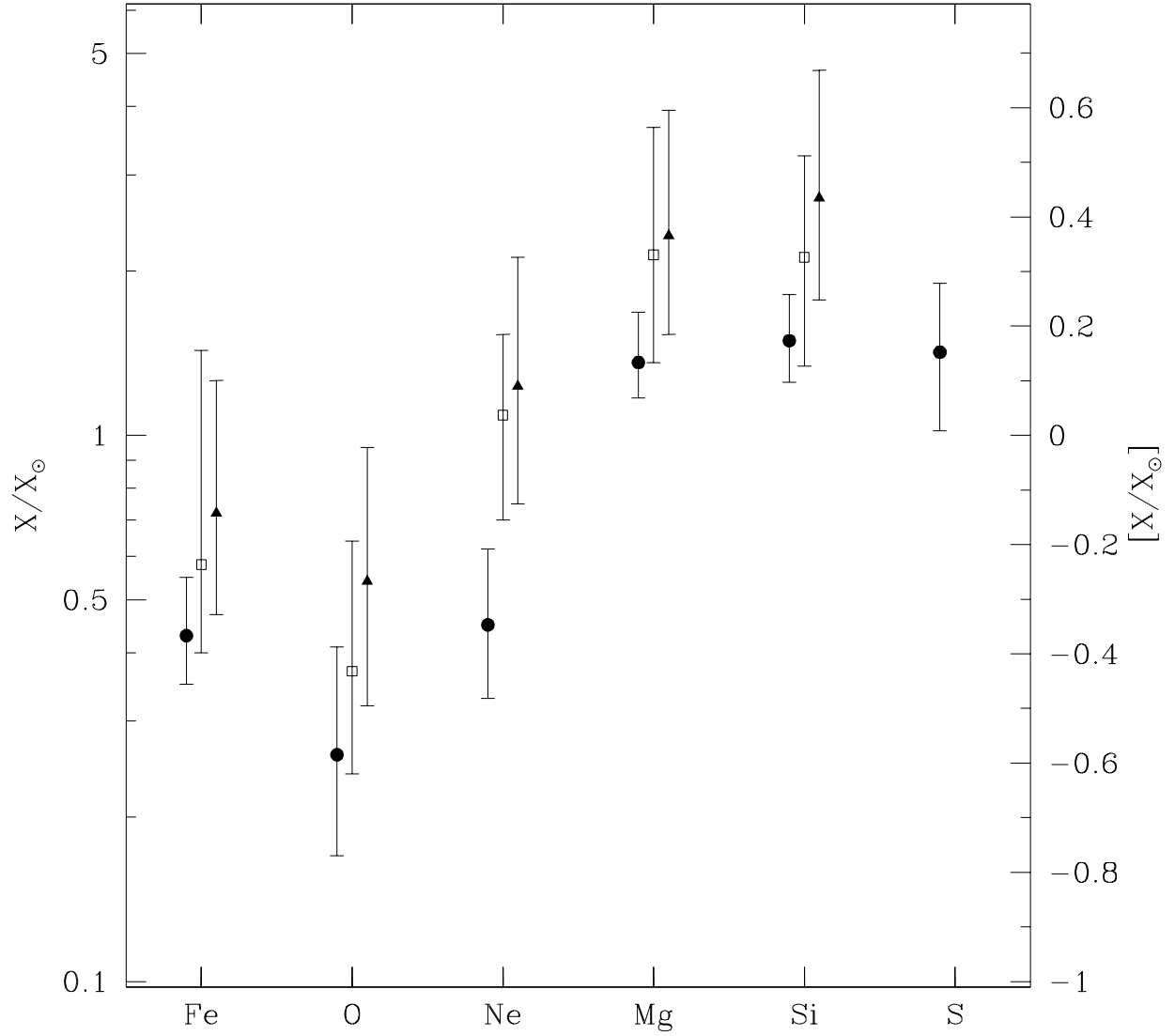


Fig. 5. Best-fit element abundances of the hot gas for different models. Filled circles: fit of both RGS and pn data, thermal plus power-law model. Open squares: RGS data alone, thermal plus power-law model. Filled triangles: RGS data alone, thermal model alone. For ease of reading the y-axis is shown both in linear and logarithmic scale.

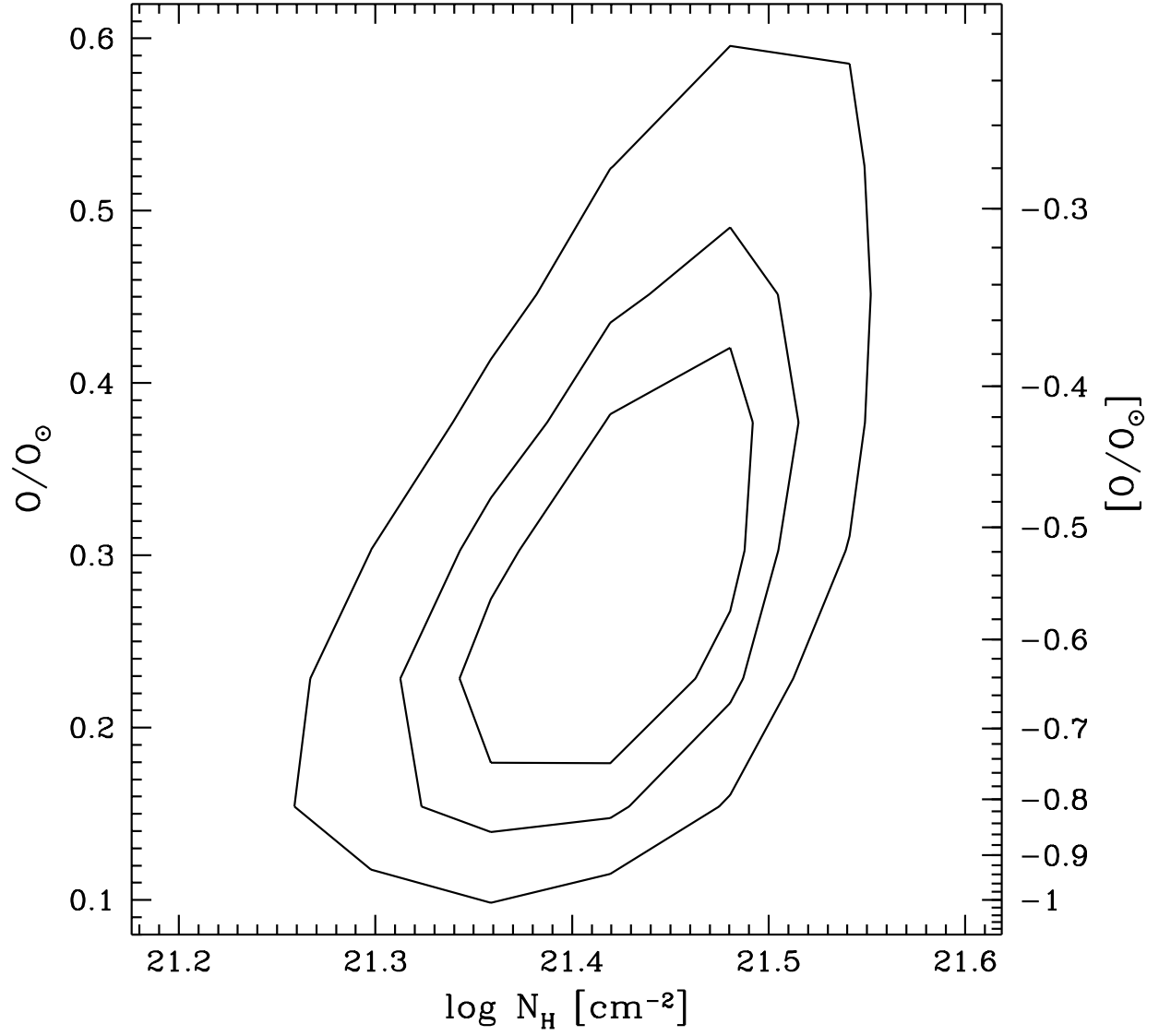


Fig. 6. Hot gas-phase oxygen abundance vs absorption. For easy of reading the y-axis is shown both in linear and logarithmic scale. The correlation, if any, is rather weak, and the oxygen abundance can be well constrained.

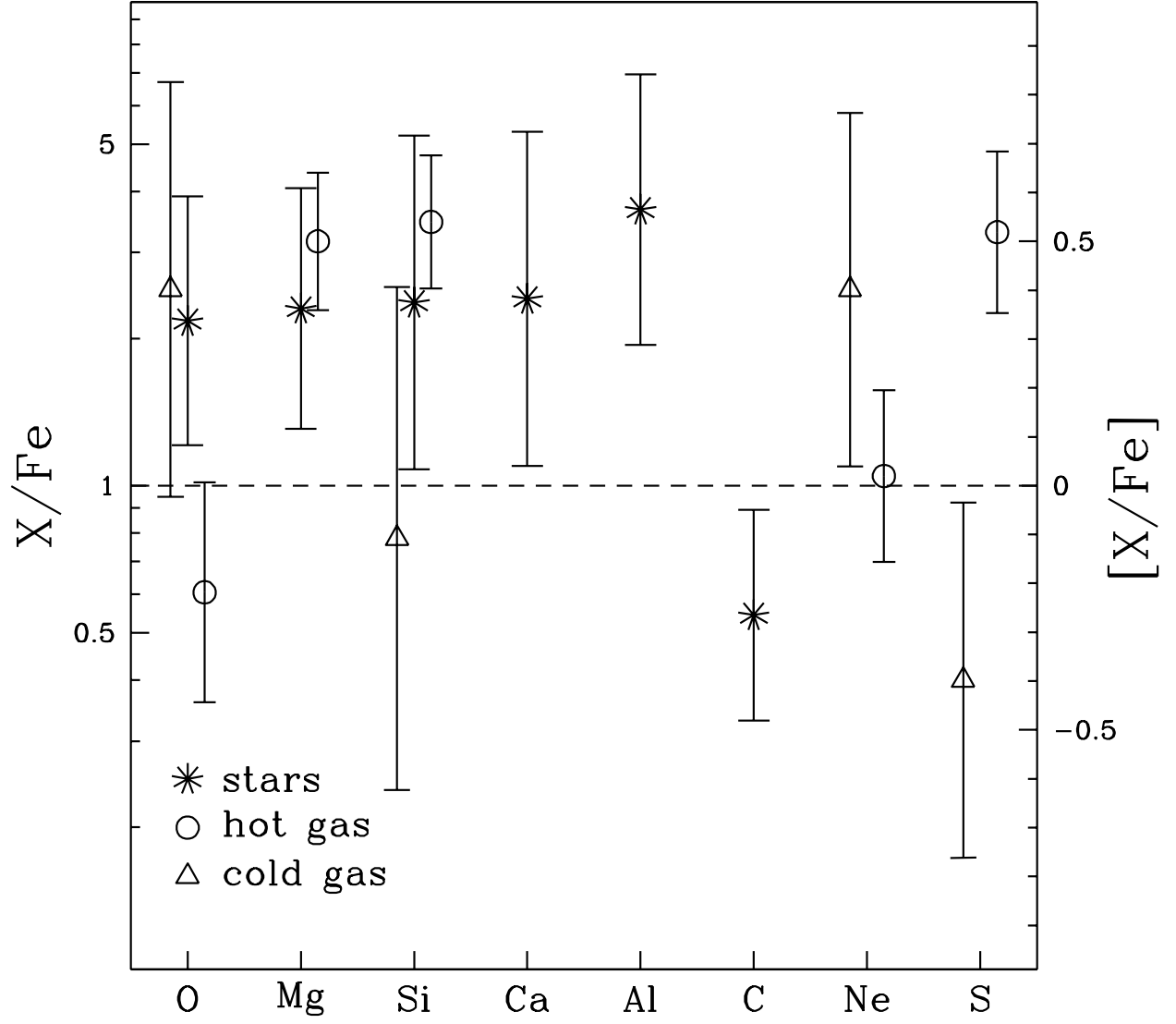


Fig. 7.] Stellar, hot and cold gas abundance ratios relative to Iron. Cold gas-phase abundances are from different data sets in the literature, hence they are not homogeneously determined. The dashed line indicates the solar values. For easy of reading the y-axis is shown both in linear and logarithmic scale.

## 5. Discussion

In M 82 all the three components, namely hot and cold gas-phases and stars trace a very similar Iron abundance, the average value being  $[\text{Fe}/\text{H}] = 0.35$  dex. Indeed, since Iron is mainly produced by SNe Ia, it is expected to be released in the ISM only after  $\sim 1$  Gyr from the local onset of SF.

At variance, elements (O, Ne, Mg, Si, S, Ca, Ti) are predominantly released by SNe II with massive progenitors on much shorter timescales. Stars trace an average  $[\text{Si}, \text{Mg}, \text{Ca}] / [\text{Fe}] = 0.4$  dex, while the hot gas suggests an average  $[\text{Si}, \text{Mg}, \text{S}] / [\text{Fe}] = 0.5$  dex. Such an overall  $[\text{O}/\text{Fe}]$  enhancement in M 82 is fully consistent with a standard chemical evolution scenario, where the ISM in the nuclear regions of massive SB galaxies is mainly enriched by the products of SNe II explosions (see e.g. Amati 1995 for a review) occurring in recursive bursts of SF of relatively short duration.

Fig. 7 shows the various abundance ratios relative to Iron, as measured in stars, hot and cold gas-phases. Since the cold gas-phase abundances are from different data sets in the literature, hence not homogeneously determined, the inferred abundance ratios should be regarded with caution.

When comparing the hot and cold gas-phase abundances, one finds Ne over-abundant, Si and especially S significantly under-abundant in the cold gas. Forster Schreiber et al. (2001) suggests S and to a lower level Si depletion onto interstellar dust grains. However, other metals like Fe in particular, with even higher degree of incorporation into dust (Savage & Sembach 1996), should be severely depleted in the cold gas, which does not seem the case. A possible explanation is that the optical lines used to infer Fe and O abundances (Albin, Collin-Soulin, & Joly 1979) and the thermal/far IR lines used to infer Ne and S abundances (Lord et al. 2001; Forster Schreiber et al. 2001) trace different nebular sub-structures within the central few hundreds pc, somewhat chemically dishomogeneous or with different dust content.

The  $[\text{O}/\text{Fe}]$  abundance ratio in M 82 is even more puzzling to interpret. Before the onset of the current burst of SF, the ISM was enriched in O as well as in the other  $\alpha$ -elements, as suggested by our stellar and cold gas-phase abundances. The O under-abundance measured in the hot gas cannot be modeled with a standard nucleosynthesis from the present generation of SNe II. Umeda et al. (2002) suggested explosive nucleosynthesis in core-collapse hypernovae but they predicted a large under-abundance of Ne and Mg as well, which is not observed.  $[\text{O}/\text{Fe}]$  under-abundance can be also explained with a major Fe enrichment by current SNe Ia explosions from previous generations of stars, but in this case all the  $[\text{O}/\text{Fe}]$  ratios should be low, again contrary to what observed. O might be also locked into dust

grains. Indeed, SNe II are known to produce significant amounts of dust (Todini & Ferrara 2001) and O, being a basic constituent of dust grains, is expected to suffer of severe dust depletion. However, other metals like Fe in particular, but also Si and Mg should be depleted into dust (Savage & Sembach 1996), leaving almost unchanged or eventually further enhancing the  $[\text{O}/\text{Fe}]$  ratio.

## 6. Conclusions

Our abundance analysis of the stellar and hot gas-phase components in the nuclear region of M 82 indicate an Iron abundance about half Solar and an overall enhancement by a factor between 2 and 3 with respect to Iron.

These abundance patterns can be easily explained within a standard nucleosynthesis scenario where the ISM is mainly enriched by SNe II on relative short timescales and with a star formation process occurring in recursive bursts.

Oxygen behaves in a strange fashion. It is over-abundant in stars and cold gas, similarly to the other  $\alpha$ -elements, while is significantly under-abundant in the hot gas. Major calibrations and/or modeling problems seem unlikely. Hypernovae nucleosynthesis, dust depletion, SNe Ia enrichment can somehow explain an Oxygen under-abundance but other metals should follow the same pattern, while they do not.

Somewhat exotic threshold effects and/or depletion mechanisms preferentially affecting Oxygen could be at work in the nuclear region of M 82, but presently this issue remains controversial.

The financial support by the Agenzia Spaziale Italiana (ASI) is kindly acknowledged.

## REFERENCES

- Allain, D., Collin-Souffrin, S., & Joly, M. 1979, *A & A*, 37, 361
- Amendt, D. 1995, *ARA & A*, 33, 115
- Biemont, E., & Grevesse, N. 1973, *Atomic Data and Nuclear Data Tables*, 12, 221
- Cappi M., Persic M., Bassani L. et al. 1999, *A & A* 350, 777
- Coziol, R., Reyes, R. E. C., Considere, S., Davoust, E., & Contini, T. 1999, *A & A*, 345, 733

- Dahlem M., Weaver K. A. & Heckman T. M. 1998, *ApJS* 118, 401
- Dahlem M., Parmar A., Osterbroek T., Orr A. et al. 2000, *ApJ* 538, 555
- Dopita, M. A., & Evans, I. M. 1986, *ApJ*, 307, 431
- Fabbiano G. 1989, *ARA & A* 27, 87
- Forster Schreiber, N. M., Genzel, R., Lutz, D., Kunze, D., & Sternberg, A. 2001, *ApJ*, 552, 544
- Frogel, J. A., Stephens, A. W., Ramirez, S., & DePoy, D. L. 2001, *AJ*, 122, 1896
- Gailey, N. I., Lester, D. F., & Telesco, C. M. 1993, *ApJ*, 407, L57
- Grevesse, N., & Sauval, A. J. 1998, *Space Science Reviews*, 85, 161
- Golla, G., Allen, M. L., & Kronberg, P. P. 1996, *ApJ*, 473, 244
- Henry, R. B. C., Edmunds, M. G., & Koppen, J. 2000, *ApJ*, 541, 660
- Johnson, H. R., Benat, A. P., & Knapp, B. M. 1980, *ApJS*, 42, 501
- Joyce, R. R., Hinkle, K. H., Wallace, L., Dulick, M., & Lambert, D. L. 1998, *AJ*, 116, 2520
- Keller, S. C. 1999, *AJ*, 118, 889
- Kleinmann, S. G., & Hall, D. N. B. 1986, *ApJS*, 62, 501
- Lord, S. D., Hollenbach, D. J., Haas, M. R., Rubin, R. H., Colgan, S. W. J., & Erickson, E. F. 1996, *ApJ*, 465, 703
- Martin, C. L., Kobulnicky, H. A., & Heckman, T. M. 2002, *ApJ*, 574, 663
- McCall, M. L. 1984, *MNRAS*, 208, 253
- McGough, S. S. 1991, *ApJ*, 380, 140
- Maeder, A., & Conti, P. S. 1994, *ARA & A*, 32, 227
- McWilliam, A. 1997, *ARA & A*, 35, 503
- Melez, J., & Barbuy, B. 1999, *ApJS*, 124, 527
- Olive, E., & Origlia, L. 1998, *A & A*, 332, 46
- Olive, E., Origlia, L., Maiolino, R., & Moorwood, A. F. M. 1999, *A & A*, 350, 9

- O riglia, L ., M oorwood, A .F .M ., & O liva, E . 1993, A & A , 280, 536
- O riglia, L ., Ferraro, F .R ., Fusi Pecci, F ., & O liva, E . 1997, A & A , 321, 859
- O riglia, L ., Goldader, J .D ., Leitherer, C ., Schaerer, D ., O liva, E . 1999, ApJ, 514, 96
- O riglia, L ., & O liva, E . 2000, NAR , 44, 257
- O riglia, L ., Rich, R .M ., & Castro, S . 2002, AJ, 123, 1559
- O riglia, L . 2003, in ASP Conf. Ser., CNO in the Universe, ed. C . Charbonnel, D . Schaerer, & G . Meynet, 203
- O riglia, L ., Ferraro, F .R ., Bellazzini, M . & Pancino, E . 2003, ApJ, 591, 916
- Pagel, B .E .J ., Edmunds, M .G ., Blackwell, D .E ., Chun, M .S ., & Smith, G . 1979, MNRAS, 189, 95
- Persic M . & Rephaeli Y . 2002, A & A 382, 843
- Ptak, A ., Serlemitsos, P ., Yaqoob, T ., Mushotzky, R ., & Tsuru, T . 1997, AJ, 113, 1286
- Ptak A . & Gri ths R . 1999, ApJ 517, L85
- Read, A .M ., & Stevens, I .R . 2002, MNRAS, 335, L36
- Rechi, S ., Matteucci, F ., & D'Ercolo, A . 2001, MNRAS, 322, 800
- Rephaeli Y . & Gruber D . 2002, A & A 389, 752
- Rieke, G .H ., Lebofsky, M .J ., Thompson, R .I ., Low, F .J ., & Tokunaga, A .T . 1980, ApJ, 238, 24
- Peimbert, M ., & Spinrad, H . 1970, ApJ, 160, 429
- Savage, B .D ., & Sembach, K .R . 1996, ARA & A , 34, 279
- Stasinska, G . 2001, Ap&SS, 277, 189
- Storchi-Bergmann, T ., Calzetti, D ., & Kinney, A .L . 1994, ApJ, 429, 572
- Strickland, D .K ., Heckman, T .M ., Weaver, K .A ., Hoopes, C .G ., & Dahlem, M . 2002, ApJ, 568, 689
- Tenorio-Tagle, G . 1996, AJ, 111, 1641

Todini, P., & Ferrara, A. 2001, *MNRAS*, 325, 726

Umeda, H., Nomoto, K., Tsunoi, T. G., & Matsumoto, H. 2002, *ApJ*, 578, 855

Wallace, L. & Hinkle, K. 1997, *ApJS*, 111, 445

Wills, K. A., Pedlar, A., Muxlow, T. W. B., & Stevens, I. R. 1999, *MNRAS*, 305, 680